Adolfo Foriero[1], Zeinab Bayati[2]

THREE DIMENSIONAL FEM BUCKLING ANALYSES OF PILES EMBEDDED IN VARIOUS SOIL TYPES

ANALIZA IZVIJANJA STUBOVA UKOPANIH U RAZNIM VRSTAMA TLA PRIMENOM TRODIMENZIONALNE MKE

Originalni naučni rad / Original scientific paper
UDK /UDC: 624.012.45.072.2.04: 519.673

Rad primljen / Paper received: 12.09.2018

Adresa autora / Author's address:
[1)] Université Laval, Faculty of Civil Engineering, Québec, Canada, Adolfo.Foriero@gci.ulaval.ca
[2)] Université Laval, Faculty of Civil Eng., Québec, Canada

Keywords
- steel pile
- buckling analysis
- pile-soil interaction
- finite element analysis
- interface elements

Abstract

Generally, piles are slender structural elements that transfer the vertical and horizontal structural loads to stiffer soil deposits or bedrock. In particular, the axial load transfer is through the pile shaft and/or via the pile end. These piles are defined as friction or end bearing piles when one of the two previously mentioned load transfers are negligible with respect to one another. This paper considers the influence of the pile head restraint, as well as lateral soil support, on the stability of axially loaded piles. This is commonly referred to as pile buckling.

Ključne reči
- čelični stub
- analiza izvijanja
- interakcija stub-tlo
- analiza konačnim elementima
- granični elementi

Izvod

Generalno, stubovi su vitki konstrukcioni elementi koji prenose vertikalno i horizontalno opterećenje konstrukcije na kruti sastav tla ili stena. Posebno, aksijalno opterećenje se prenosi kroz osovinu stuba i/ili na kraj stuba. Ovi stubovi se definišu kao frikcioni, ili sa osloncem na kraju stuba, kada je jedan od prethodna dva tipa prenosa opterećenja zanemarljiv, jedan u odnosu na drugi. U radu se razmatra uticaj ograničenog pomeranja vrha stuba, kao i bočno oslanjanje u tlu, na stabilnost aksijalno opterećenih stubova. Ovakvo ponašanje se često naziva izvijanje stuba.

INTRODUCTION

Pile buckling is a particular type of structural failure. However, the critical buckling load depends on various factors such as: (1) the pile section properties (length, cross-section, elastic material properties); (2) the type of soil confining the pile (sand and/or clay); (3) the type of stress analyses (effective stress analysis (ESA) for long term conditions or total stress analyses (TSA) for short term conditions); and (4) the method of pile installation. In this paper, all four points are covered to a certain degree, except that for the third point, the analysis is restricted to long-term conditions only (elastic drained soil moduli). Moreover, this study considers a pile having a box cross-section, where the method of installation is generally by pile driving.

There are various studies in the literature on buckling. In particular, buckling is a dominant failure mode for slender piles in very soft clays /1, 4, 11/, loose sands and soils defined as liquefiable /2, 3, 7, 12/. The buckling failure of piles, in these studies, is primarily caused by the effect of the axial load inducing a loss of lateral support on the surrounding soil.

An important transgression is warranted at this point. One example of extreme and drastic condition, leading to the lateral loss of support is when the surrounding soil liquefies. This occurs in liquefiable soils, such as saturated sands and silts, when subject to cyclic loading. The pore pressure build up in such conditions leads to a complete loss of the confining effective stress and thus the soil offers no lateral support. Consequently, in liquefiable soils, piles should be designed with no account for lateral support and furthermore, the pile end should be extended to bedrock or to extremely stiff soils /10/. In fact, a pile embedded in a liquefiable soil is literally designed as an elastic column.

A recent example of piles constructed in liquefiable soils is the 58-story (197-meter-tall) Millennium Tower in San Francisco. The piled foundation includes 950 cylinder concrete friction piles (18 to 27-meter-deep). This type of construction led the tower to sink 0.44 m and tilt 0.36 m towards the northwest, since completion of construction in 2008. The main reason for the excessive soil deformation leading to the instability of the Tower is not clearly understood. However, because the Millennium tower rests on a liquefiable soil deposit, and because the San Francisco region is at high risk for tremors, the piles should be extended to bedrock and designed for buckling. The case of the Millennium Tower constitutes an extreme or albeit exception of piled foundations.

The circumstances are different when piles are embedded or partially embedded in non-liquefiable soils. In those cases, one can rely on the shaft as well as end bearing resistance of the surrounding soil. This is a shared view of many researchers in the geotechnical field. However, a common practice is to assume the end of the pile to be fixed /6, 8, 9, 13-15/. This assumption is restrictive because even in very stiff soil deposits, the possibility of pile tip settle-

ment and rotation cannot be excluded. Consequently, the pile tip should be modelled as a free end, embedded in a stable surrounding soil medium, which gradually extends to distances where stresses and strains are negligible.

Consequently, the present study considers a three dimensional analysis of the linear elastic critical buckling load of a steel box-section pile embedded in various soil deposits. The embedded end of pile is modelled as free. In practice, pile groups are capped and consequently when analysing a single pile one must consider the type of restraint condition imposed on the pile head and whether or not the pile section is only partially embedded. Detail of the FEM modelling encompassing these facts are given at a later section.

Finally, curves illustrating the factors affecting the numerically calculated critical buckling loads are presented. The 3D FEM simulations, yielding these curves, require as input the pile section elastic properties, as well as the elastic drained properties of the surrounding soil. These behavioural curves are obtained for different pile head restraints in various soils, and so there is no need to address the pile end condition since the pile end is modelled as free.

BUCKLING OF PARTIALLY EMBEDDED BOX-SECTION PILES IN A 3-D ELASTIC CONTINUUM

The stability or buckling of a pile leads to an eigenvalue problem. As previously mentioned, studies in the past modelled the problem as that of an embedded beam-column subjected to an axial compressive stress. The soil reaction as provided by either a Winkler or Elastic continuum were an integral part of the governing partial differential equation for the pile section. Therefore, two boundary conditions (at the pile head and tip) were necessary in order to determine the eigenvalues. However, this approach (modelling buckling as a beam-column) renders the boundary condition at the pile end rather restrictive.

This study challenges the problem differently and encompasses the following assumptions:

– The pile and surrounding soil are sub-domains of an elastic three-dimensional continuum.
– The elastic material properties of both the pile section (E_p, μ_p) and soil (E'_s, μ'_s) are homogeneous and isotropic.
– The pile-soil interface is modelled as thin elastic continuum having a stiffness in both the normal and tangential direction to shear.
– In the calculation of the critical buckling load, only the pile head is subject to kinematic constraints.
– The ensuing FEM analyses consider geometric nonlinearity for both the pile and surrounding soil.

The sole kinematic constraint (concerning the pile section) imposed in the FEM analyses are that of a hinged or free pile head. Generally, these conditions depend on the pile head's fixity with respect to a pile cap and on the unsupported length of the pile. One cannot overemphasize that no kinematic constraints are necessary at the pile tip because the analyses are three dimensional (the surrounding soil stabilizes the embedded portion of the pile), not to mention the degree of fixity that is difficult to ascertain.

However, when one deals with a geometrically nonlinear behaviour such as buckling, a state is established in which changes in geometry have a significant effect on the resulting load-displacement characteristics of a solid body. When geometric changes are significant, the geometry of the body must be updated continuously to determine the new position of a material point. Hence, in a large deformation analysis, one must consider that the configuration of a body is changing unremittingly. This fact is very different from linear finite element analyses where displacements are infinitely small so that the configuration of the body does not change.

TOTAL LAGRANGIAN FORMULATION

In order to deal with continuous changes in configurations, one must choose the appropriate stress and strain measures. One possibility of stress and strain measures which fulfil this requirement is the 2nd Piola-Kirchhoff stress tensor and the Green-Lagrange strain tensor which are a compatible conjugate energy pair. It can be shown that the second Piola-Kirchhoff stress tensor S is work-conjugate to the rate of Green-Lagrange strain tensor $\dot{E}$:

$$W = \frac{1}{2}\int_V S\dot{E}dV \,. \tag{1}$$

In other words, the equations of motion must now be derived for the deformed configuration of the soil-structure system at time t. Since the geometry of the deformed configurations is unknown, the equations must be rewritten in terms of a reference configuration. One of the key quantities to attain this objective is the deformation gradient tensor F which gives the relationship of a material line dX (material or Lagrangian differential element) before deformation to the line dx after deformation (spatial or Eulerian differential element). The deformation gradient tensor is defined in terms of the Lagrangian and Eulerian coordinates as

$$F = \left(\frac{\partial x}{\partial X}\right)^T \equiv (\Delta_o x)^T \,, \tag{2}$$

and gives rise to the symmetric Green-Lagrange strain tensor

$$E = \frac{1}{2}(F^T \cdot F - I) = \frac{1}{2}\left[(\nabla_o u)^T + \nabla_o u + (\nabla_o u)^T \cdot \nabla_o u\right]. \tag{3}$$

The second Piola-Kirchhoff stress tensor S is used in the total Lagrangian formulation of a geometrically nonlinear analysis by considering the transformation of the current force df on a deformed elemental area da to the force dF on the undeformed area dA. This stress, S, is given as

$$dF = F^{-1} \cdot df \equiv dA \cdot S \,. \tag{4}$$

Thus, the second Piola-Kirchhoff stress tensor gives the transformed current force per unit undeformed area. The relationship between the usual *Cauchy stress tensor*, σ (current configuration), and second Piola-Kirchhoff stress tensor S is given as

$$S = JF^{-1} \cdot \sigma \cdot F^{-T} \,, \tag{5}$$

where: J stands for the Jacobian of the transformation or the determinant of the deformation gradient matrix

$$J = |F| \,. \tag{6}$$

In the total Lagrangian formulation all quantities in the current configuration C_i are measured with respect to the initial configuration, from herein identified as the reference configuration $C_R = C_0$, where one considers the collection of intermediate configurations as (C_0, C_1, C_2, …, C_{i-1}).

For the total Lagrangian formulation, the elastic constitutive equations are expressed in terms of the Kirchhoff stress increment tensor components ${}_0S_{ij}$ and Green-Lagrange strain increment tensor component ${}_0\varepsilon_{kl}$ through the material elasticity tensor C as

$$ {}_0S_{ij} = {}_0C_{ijkl}\ {}_0\varepsilon_{kl}\,, \tag{7} $$

$$ {}^{i}_{0}S_{ij} = {}^{i-1}_{0}S_{ij} + {}_0S_{ij}\,, \tag{8} $$

and

$$ {}^{i}_{0}E_{ij} = {}^{i-1}_{0}E_{ij} + {}_0\varepsilon_{ij}\,, \tag{9} $$

where ${}_0{}^{i}S_{ij}$ and ${}^{i-1}{}_0S_{ij}$, and ${}_0{}^{i}E_{ij}$ and ${}^{i-1}{}_0E_{ij}$, are respectively the second Piola-Kirchhoff stress tensor and the Green-Lagrange strain tensor components in the C_i and C_{i-1} configurations.

In the total Lagrangian formulation, the weak form is given as

$$ \int_{{}_0V} {}^{2}_{0}S_{ij}\,\delta({}^{2}_{0}E_{ij})\,d\,{}^{0}V - \delta({}^{2}_{0}R) = 0\,, \tag{10} $$

where

$$ {}^{2}_{0}S_{ij} = {}^{2}_{0}J\left(\frac{\partial\,{}^{0}x_i}{\partial^{2}x_m}\right)^{2}\sigma_{mn}\left(\frac{\partial\,{}^{0}x_j}{\partial^{2}x_n}\right), $$

$$ {}^{2}_{0}E_{ij} = \frac{1}{2}\left(\frac{\partial^{2}_{0}u_i}{\partial\,{}^{0}x_j} + \frac{\partial^{2}_{0}u_j}{\partial\,{}^{0}x_i} + \frac{\partial^{2}_{0}u_k}{\partial\,{}^{0}x_i}\frac{\partial^{2}_{0}u_k}{\partial\,{}^{0}x_j}\right), \tag{11} $$

and

$$ \delta({}^{2}_{0}R) = \int_{{}_0V} {}^{2}_{0}f_i\,\delta u_i\,d\,{}^{0}V + \int_{{}_0S} {}^{2}_{0}t_i\,\delta u_i\,d\,{}^{0}S\,. \tag{12} $$

For computational purposes the incremental decomposition of this weak form is rewritten as

$$ \int_{{}_0V} {}_0S_{ij}\,\delta({}_0\varepsilon_{ij})\,d\,{}^{0}V + \int_{{}_0V} {}^{1}_{0}S_{ij}\,\delta({}_0\eta_{ij})\,d\,{}^{0}V = $$
$$ = \delta({}^{2}_{0}R) - \int_{{}_0V} {}^{1}_{0}S_{ij}\,\delta({}_0e_{ij})\,d\,{}^{0}V \tag{13} $$

where

$$ {}_0e_{ij} = \frac{1}{2}\left(\frac{\partial u_i}{\partial\,{}^{0}x_j} + \frac{\partial u_j}{\partial\,{}^{0}x_i} + \frac{\partial\,{}^{1}_{0}u_k}{\partial\,{}^{0}x_i}\frac{\partial u_k}{\partial\,{}^{0}x_j} + \frac{\partial u_k}{\partial\,{}^{0}x_i}\frac{\partial\,{}^{1}_{0}u_k}{\partial\,{}^{0}x_j}\right), \tag{14} $$

$$ {}_0\eta_{ij} = \frac{1}{2}\frac{\partial u_k}{\partial\,{}^{0}x_i}\frac{\partial u_k}{\partial\,{}^{0}x_j}\,, \tag{15} $$

and

$$ {}_0\varepsilon_{ij} = {}_0e_{ij} + {}_0\eta_{ij}\,. \tag{16} $$

Finally, the total Lagrangian formulation in matrix notation is given as

$$ \left([K_L] + [K_{NL}]\right)\{\overline{\Delta}\} = \left\{{}^{2}_{0}F\right\} - \left\{{}^{1}_{0}F\right\}, \tag{17} $$

where

$$ [K_L] = \int_{{}_0V} [B_L]^{T}\,[{}_0C]\,[B_L]\,d\,{}^{0}V\,, \tag{18} $$

$$ [K_{NL}] = \int_{{}_0V} [B_{NL}]^{T}\,[{}^{1}_{0}S]\,[B_{NL}]\,d\,{}^{0}V\,, \tag{19} $$

$$ \left\{{}^{1}_{0}F\right\} = \int_{{}_0V} [B_L]^{T}\left\{{}^{1}_{0}S\right\} d\,{}^{0}V\,, \tag{20} $$

$$ \left\{{}^{2}_{0}F\right\} = \int_{{}_0V} [\psi]^{T}\left\{{}^{2}_{0}f\right\} d\,{}^{0}V + \int_{{}_0S} [\psi]^{T}\left\{{}^{2}_{0}t\right\} d\,{}^{0}S\,, \tag{21} $$

$$ \left\{{}^{2}_{0}f\right\} = \begin{Bmatrix} {}^{2}_{0}f_x \\ {}^{2}_{0}f_y \end{Bmatrix}, \quad \left\{{}^{2}_{0}t\right\} = \begin{Bmatrix} {}^{2}_{0}t_x \\ {}^{2}_{0}t_y \end{Bmatrix}. \tag{22} $$

BUCKLING ANALYSIS IN THE CONTEXT OF THE TOTAL LAGRANGIAN FORMULATION

A linearized buckling analysis considers a linear eigenvalue approach to the nonlinear problem. Namely, the buckling criterion is fulfilled when the displacements are indeterminate, or the stiffness matrix is singular. As previously derived (Eqs.(18) and (19)), the total stiffness matrix for the full geometrically nonlinear problem $[K]$ is the sum of two contributions

$$ [K] = \left([K_L] + [K_{NL}(P)]\right), \tag{23} $$

where $[K_L]$ is the ordinary stiffness matrix for the linear case, whereas $[K_{NL}(P)]$ is the nonlinear component which depends on the load P.

One can linearly approximate the previous expression, Eq.(23), by considering that K_{NL} is proportional to the loading P_0, thus yielding

$$ [K] = \left([K_L] + \lambda[K_{NL}(P_o)]\right). \tag{24} $$

The result is an eigenvalue problem for the parameter λ given by

$$ \left([K_L] + \lambda[K_{NL}(P_o)]\right)u = 0\,. \tag{25} $$

Then the lowest eigenvalue λ is the critical load factor of the pile-soil system, and the corresponding Eigen mode, **u**, gives the associated buckling shape of the pile.

DISCUSSION OF FINITE ELEMENT SIMULATION RESULTS

The analyses of the buckling problem are carried out by assuming a three dimensional continuum that incorporates both the box-section pile (Fig. 1) and the surrounding soil (Figs. 2 and 3). Finite element simulations are carried out by commercial software COMSOL 5.3, /5/. One also deciphers in these figures the use of infinite elements in order to eliminate possible boundary effects. As shown in these figures, a typical finite element mesh is constituted with tetrahedral elements, totalling 32000 degrees of freedom.

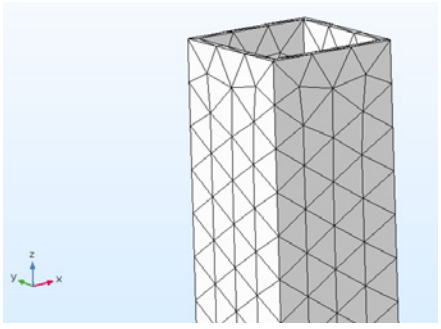

Figure 1. The box section of piles in finite element analyses.

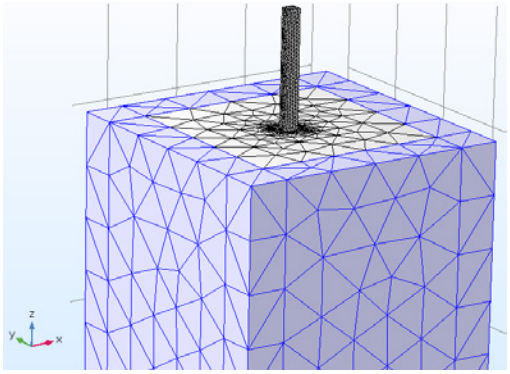

Figure 2. Partially embedded pile in soil.

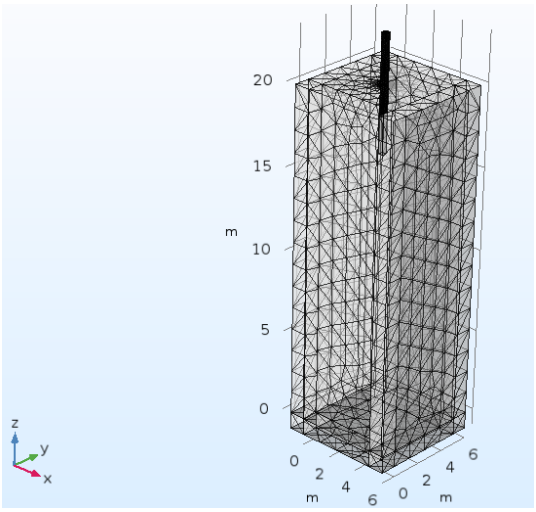

Figure 3. Finite element model of the pile-soil system.

The pile and surrounding soil are theoretical subdomains with their respective linear elastic properties. These subdomains interact through thin layer elastic interface elements. These elements are necessary in order to establish a frictional interface between the pile and surrounding soil. Moreover, because these thin layer elements are used to model interface friction only, they must be constrained against any possible volume change. This is best achieved by assuming a very high stiffness of the thin layer element perpendicular to the shearing direction.

In all of the simulations, no assumptions of fixity of the pile tip are realized. In other words, the pile tip is modelled to be free of movement or completely unrestrained.

A total of 500 simulations are carried out in order to calculate the critical buckling load of the soil-pile system λP_0 and to basically extract from the analysis the associated pile mode shape. The elastic properties of pile material and various soil types (drained conditions) used in the finite element analyses are shown in Table 1.

Table 1. Elastic properties of pile material and soils.

Soil type	$E's$ (MPa)	$\mu's$
Soft clay	10	0.38
Medium clay	25	0.33
Stiff clay	65	0.25
Loose sand	15	0.2
Medium sand	30	0.28
Dense sand	60	0.3
Pile material (steel)	E_p = 200 GPa	μ_p = 0.33

Typical results of the analyses are presented in Tables 2 to 13. Tables 2 to 4 provide the FEM critical buckling load factors for a pile embedded respectively in a soft, medium and stiff clay, having a non-clamped pile head. These results demonstrate that critical buckling load increases with embedment, and for a constant unsupported length of pile. These results are shown in Fig. 4, where the FEM critical buckling load is plotted as a function of the slenderness ratio.

Table 2. Critical buckling load factors for a non-clamped pile head in soft clay (perfectly rough soil-pile interface).

pile slenderness	L_u (m)	L_e (m)	critical buckling load factor
L/D = 17.14	3.0	3.0	4.6424e6
L/D = 14.28	3.0	2.0	3.0177e6
L/D = 11.43	3.0	1.0	1.0102e6
L/D = 10	3.0	0.5	3.3312e5

Table 3. Critical buckling load factors for a non-clamped pile head in medium clay (perfectly rough soil-pile interface).

pile slenderness	L_u (m)	L_e (m)	critical buckling load factor
L/D = 17.14	3.0	3.0	6.3202e6
L/D = 14.28	3.0	2.0	5.2788e6
L/D = 11.43	3.0	1.0	2.2897e6
L/D = 10	3.0	0.5	8.0917e5

Table 4. Critical buckling load factors for a non-clamped pile head in stiff clay (perfectly rough soil-pile interface).

pile slenderness	L_u (m)	L_e (m)	critical buckling load factor
L/D = 17.14	3.0	3.0	7.5847e6
L/D = 14.28	3.0	2.0	7.3101e6
L/D = 11.43	3.0	1.0	4.6771e6
L/D = 10	3.0	0.5	1.9643e6

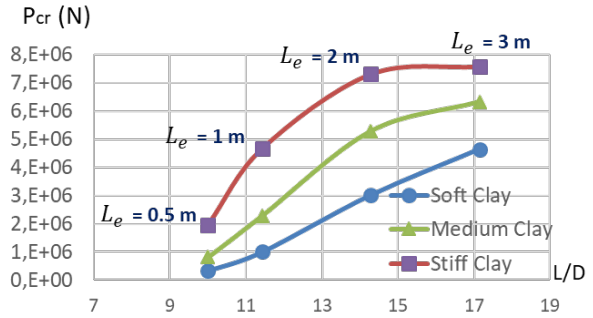

Figure 4. Critical buckling load factor vs. global slenderness ratio for non-clamped head piles in clay.

Similarly in clays, for cases when the pile head is clamped (Tables 5 to 7), the critical buckling load increases with embedment for a constant unsupported length of pile. However, the values of critical buckling load are higher and the rate of increase of P_{cr}, with respect to slenderness ratio, is more pronounced. This trend is depicted in Fig. 5.

Table 5. Critical buckling load factors for a clamped pile head in soft clay (perfectly rough soil-pile interface).

pile slenderness	L_u (m)	L_e (m)	critical buckling load factor
L/D = 17.14	3.0	3.0	6.0535e6
L/D = 14.28	3.0	2.0	4.2014e6
L/D = 11.43	3.0	1.0	2.6627e6
L/D = 10	3.0	0.5	1.6154e6

Table 6. Critical buckling load factors for a clamped pile head in medium clay (perfectly rough soil-pile interface).

pile slenderness	L_u (m)	L_e (m)	critical buckling load factor
L/D = 17.14	3.0	3.0	1.6559e7
L/D = 14.28	3.0	2.0	1.1526e7
L/D = 11.43	3.0	1.0	7.1883e6
L/D = 10	3.0	0.5	4.320e6

Table 7. Critical buckling load factors for a clamped pile head in stiff clay (perfectly rough soil-pile interface).

pile slenderness	L_u (m)	L_e (m)	critical buckling load factor
L/D = 17.14	3.0	3.0	4.9215e7
L/D = 14.28	3.0	2.0	3.419e7
L/D = 11.43	3.0	1.0	2.0829e7
L/D = 10	3.0	0.5	1.2268e7

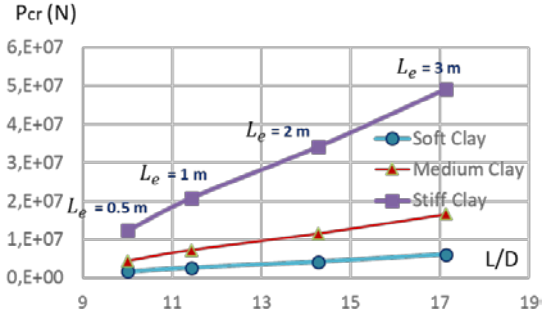

Figure 5. Critical buckling load factor vs. global slenderness ratio for clamped head piles in clay.

Tables 8 to 10 provide the FEM critical buckling load factors for a pile embedded respectively in a loose, medium and dense sand, having a non-clamped pile head. These results demonstrate that critical buckling load increases with embedment, and for a constant unsupported length of pile. These results are shown in Fig. 6, where the FEM critical buckling load is plotted as a function of the slenderness ratio.

Table 8. Critical buckling load factors for a non-clamped pile head in loose sand (perfectly rough soil-pile interface).

pile slenderness	L_u (m)	L_e (m)	critical buckling load factor
L/D = 17.14	3.0	3.0	5.5203e6
L/D = 14.28	3.0	2.0	4.1001e6
L/D = 11.43	3.0	1.0	1.5295e6
L/D = 10	3.0	0.5	5.1523e5

Table 9. Critical buckling load factors for a non-clamped pile head in medium sand (perfectly rough soil-pile interface).

pile slenderness	L_u (m)	L_e (m)	critical buckling load factor
L/D = 17.14	3.0	3.0	6.5929e6
L/D = 14.28	3.0	2.0	5.7394e6
L/D = 11.43	3.0	1.0	2.6824e6
L/D = 10	3.0	0.5	9.7032e5

Table 10. Critical buckling load factors for a non-clamped pile head in dense sand (perfectly rough soil-pile interface).

pile slenderness	L_u (m)	L_e (m)	critical buckling load factor
L/D = 17.14	3.0	3.0	7.4824e6
L/D = 14.28	3.0	2.0	7.1564e6
L/D = 11.43	3.0	1.0	4.4092e6
L/D = 10.00	3.0	0.5	1.8106e6

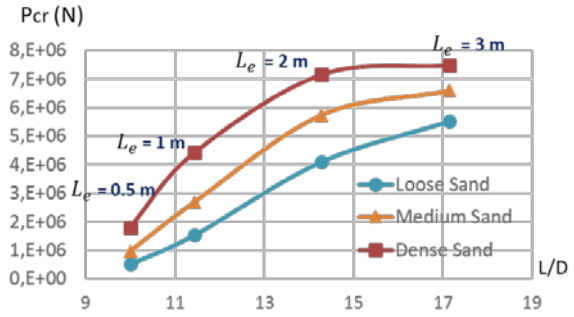

Figure 6. Critical buckling load factor vs. global slenderness ratio for non-clamped head piles in sand.

For sands, the cases when the pile head is clamped (Tables 11 to 13) also yields a critical buckling load that increases with embedment for a constant unsupported length of pile. However, values of the critical buckling load are higher and the rate of increase of P_{cr}, with respect to the slenderness ratio, is more pronounced. This trend is shown in Fig. 7.

Table 11. Critical buckling load factors for a clamped pile head in loose sand (perfectly rough soil-pile interface).

pile slenderness	L_u (m)	L_e (m)	critical buckling load factor
L/D = 17.14	3.0	3.0	1.1902e7
L/D = 14.28	3.0	2.0	8.3662e6
L/D = 11.43	3.0	1.0	5.1147e6
L/D = 10	3.0	0.5	2.9893e6

Table 12. Critical buckling load factors for a clamped pile head in medium sand (perfectly rough soil-pile interface).

pile slenderness	L_u (m)	L_e (m)	critical buckling load factor
L/D = 17.14	3.0	3.0	2.1452e7
L/D = 14.28	3.0	2.0	1.4982e7
L/D = 11.43	3.0	1.0	9.2423e6
L/D = 10	3.0	0.5	5.4736e6

Table 13. Critical buckling load factors for a clamped pile head in dense sand (perfectly rough soil-pile interface).

pile slenderness	L_u (m)	L_e (m)	critical buckling load factor
L/D = 17.14	3.0	3.0	4.2262e7
L/D = 14.28	3.0	2.0	2.9284e7
L/D = 11.43	3.0	1.0	1.8013e7
L/D = 10	3.0	0.5	1.0704e7

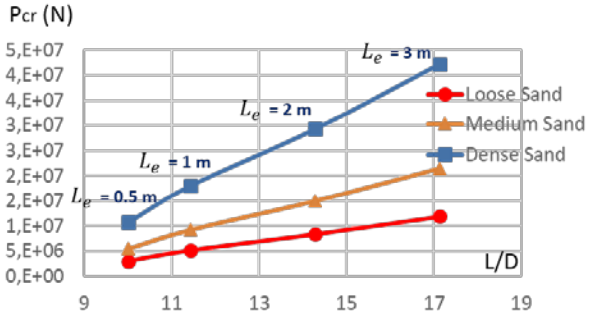

Figure 7. Critical buckling load factor vs. global slenderness ratio for clamped head piles in sand.

The previous cases just discussed, provide a limiting condition because the interface conditions are idealized as perfectly rough. However, as previously mentioned, the true interface roughness lies somewhere between the perfectly

smooth and perfectly rough cases. For this reason, the thin layer elastic interface elements are utilized to model the interface behaviour. These interface elements must be constrained in the normal direction with respect to shear, in order to limit the possibility of volume change. The following equation for a thin elastic interface element is used in the analyses

$$\begin{pmatrix} k_{11} & 0 & 0 \\ 0 & k_{22} & 0 \\ 0 & 0 & k_{33} \end{pmatrix} \cdot \begin{Bmatrix} u_{1r} \\ u_{2r} \\ u_{3r} \end{Bmatrix} = \begin{Bmatrix} F_1 \\ F_2 \\ F_3 \end{Bmatrix}, \qquad (26)$$

where: k_{11}, k_{22}, k_{33} are the interface stiffnesses per unit area [N/m^3]; u_{1r}, u_{2r}, u_{3r} are the relative displacements [m]; and F_1, F_2, F_3 represent the force per area as a function of extension [N/m^2], respectively in the x, y and z direction. In order to limit volume change, the maximal permissible machine value of k_{ii} ($1 \le i \le 3$) in the direction normal to shear is imposed. In this study, this value is taken as 1e19 N/m^3.

Typical results demonstrating the effects of the interface stiffness values for an unclamped pile in a medium clay are shown in Fig. 8.

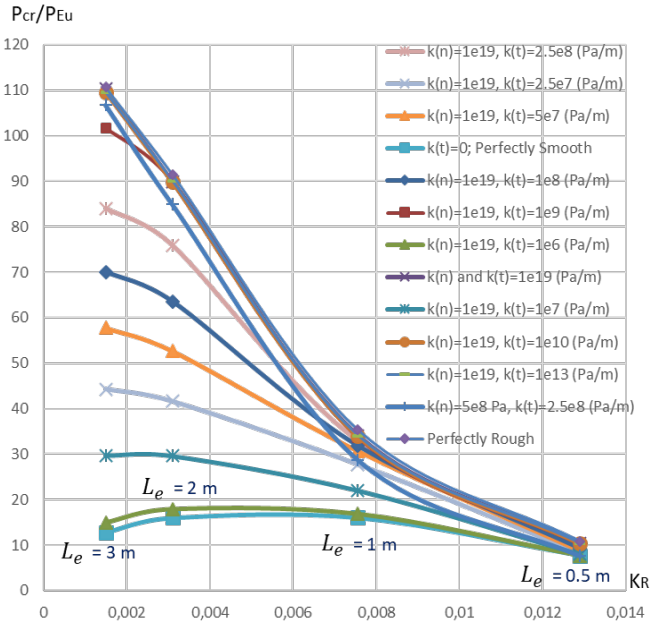

Figure 8. Bracketing the surface roughness of the elastic interface thin element for a pile embedded in medium clay.

In the above figure, the P_{cr}/P_{Eu} versus K_R ($K_R = (E_pI_p)/(E'_sL^4)$) ratios, for different pile embedment lengths, confirm that the buckling behaviour is strongly affected by interface friction. The interface friction is bracketed by assume a perfectly rough: k_t = 1e19 N/m^3, and perfectly smooth: $k_t = 0$, interface where the index t stands for the direction of shear or direction tangent to the pile surface. The value of normal stiffness in all cases is maintained as k_n = 1e19 N/m^3 in order to reduce the possibility of volume change. One cannot overstate this fact because thin layer elastic elements in COMSOL are continuum elements that are used as interface elements. The real value of the interface stiffness is lurking somewhere between the limiting bracketed values. Simulations with interface values between these two confirm this fact.

An interesting result, stemming from the present analyses is the calculation of the normalized critical buckling load P_{cr}/P_{Eu} in terms of the soil stiffness E'_s. From a practical point of view, the civil engineer must reconcile the pile with the surrounding medium. One way to achieve this is by curve fitting the nonlinear equation

$$\frac{P_{cr}}{P_{Eu}} = a_0 + a_1 e^{-\frac{E_pI_p}{E'_sL^4}} + a_2 \frac{E_pI_p}{E'_sL^4} e^{-\frac{E_pI_p}{E'_sL^4}}. \qquad (27)$$

Through the previously obtained P_{cr}/P_{Eu} versus K_R curves, for various degrees of interface friction the typical values resulting from nonlinear regression analyses are presented in Tables 14 to 17. These coefficient values are valid for a nonlinear regression using 4 points (corresponding to 4 FEM simulations). When more points or simulations are considered, the values of the coefficients change, but the overall trend or approximation is maintained.

Table 14. Values of P_{cr}/P_{Eu} -K_R fitting relationship coefficients for non-clamped piles and interface of k_n = 1e19 Pa/m and k_t = 1e10 Pa/m in clays.

	a_0	a_1	a_2
Soft clay	2.37e+05	-2.37e+05	-2.46e+05
Medium clay	1345301.184	-1.35e+06	-1.36e+06
Stiff clay	-5.96e+04	59672.91	50008.24

Table 15. Values of P_{cr}/P_{Eu}-K_R fitting relationship coefficients for non-clamped piles and interface of k_n =1e19 Pa/m and k_t = 1e10 Pa/m in sands.

	a_0	a_1	a_2
Loose sand	4.80e+05	-4.80e+05	-4.92e+05
Medium sand	887047.0675	-886935.8657	-901161.996
Dense sand	3415624.941	-3415555.894	-3432978.38

Table 16. Values of P_{cr}/P_{Eu}-K_R fitting relationship coefficients for clamped piles and interface of k_n = 1e19 Pa/m and k_t = 1e10 Pa/m in clays.

	a_0	a_1	a_2
Soft clay	-2.18e+04	2.18e+04	2.21e+04
Medium clay	-1.01e+05	1.01e+05	1.02e+05
Stiff clay	-1.49e+06	1.49e+06	1.49e+06

Table 17. Values of P_{cr}/P_{Eu}-K_R fitting relationship coefficients for clamped piles and interface of k_n = 1e19 Pa/m and k_t = 1e10 Pa/m in sands.

	a_0	a_1	a_2
Loose sand	-7.42e+04	7.42e+04	7.50e+04
Medium sand	-3.26e+05	3.26e+05	3.28e+05
Dense sand	-1.12e+06	1.12e+06	1.12e+06

For the cases where one considers an unclamped pile with a perfectly rough interface (k_t = 1e19 N/m^3, Figs. 9 and 10) in both clays and sands, the critical buckling load decreases as the stiffness of the surrounding medium decreases. A similar trend is observed in Figs. 11 and 12 but for a pile-soil interface of finite roughness or stiffness, of k_t = 1e10 N/m^3.

On the other hand, the behaviour of a clamped head pile is rather unpredictable as shown in Figs. 13 and 14 (when interface friction is imposed). For clays (Fig. 13), the results indicate that the critical buckling load initially increases in order to attain a maximal value and then decreases as a

function of surrounding soil stiffness. For a clamped pile in sand, the critical buckling load decreases with soil stiffness to then level off at near asymptotic value (Fig. 14).

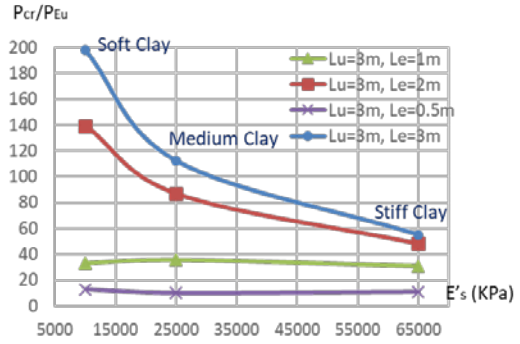

Figure 9. Buckling behaviour curves of non-clamped piles with perfectly rough interface surface in clays.

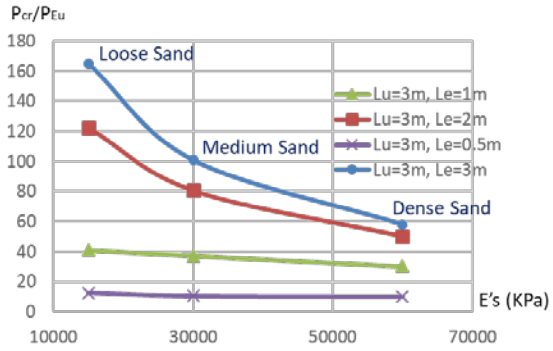

Figure 10. Buckling behaviour curves of non-clamped piles with perfectly rough interface surface in sands.

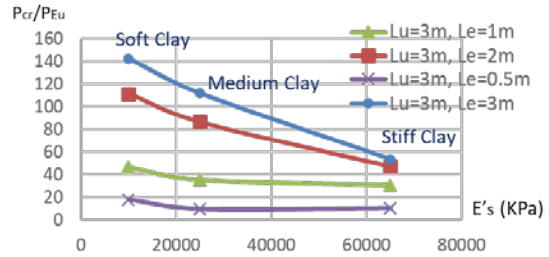

Figure 11. Buckling behaviour curves of non-clamped with interface of k_n = 1e19 Pa/m and k_t = 1e10 Pa/m in clays.

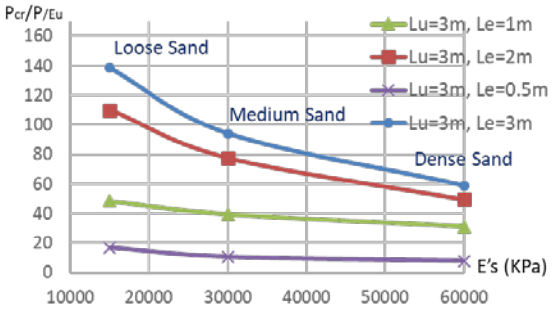

Figure 12. Buckling behaviour curves of non-clamped with interface of k_n = 1e19 Pa/m and k_t = 1e10 Pa/m in sands.

As previously mentioned, nothing guaranties that a pile end is perfectly fixed when embedded in a soil continuum, and consequently this hypothesis is investigated. It is quite clear from the FEM results shown in Figs. 15 and 16 that assuming the pile tip to be fixed in the soil, yields critical buckling loads that are much lower than the cases when the pile end is free. This fact leads to economic versus safety issues when designing the pile for the critical buckling load. If the pile is embedded in a liquefiable soil then it should be extended to bedrock, and in such a particular case, fixity of the end could be assumed.

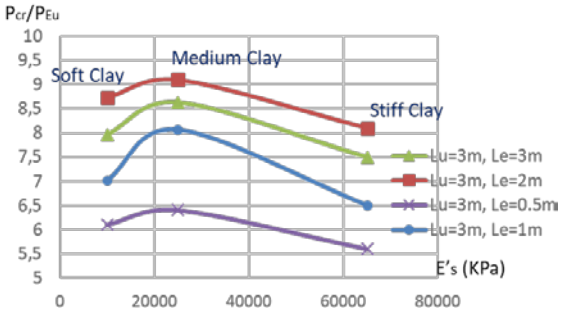

Figure 13. Buckling behaviour curves of clamped with interface of k_n = 1e19 Pa/m, and k_t = 1e10 Pa/m in clays.

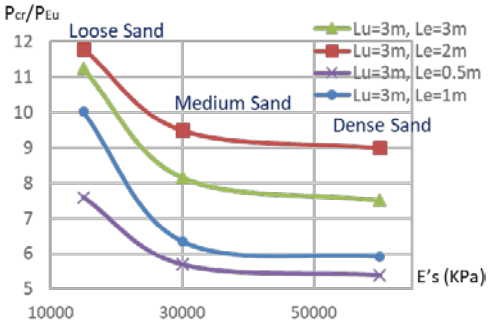

Figure 14. Buckling behaviour curves of clamped with interface of k_n = 1e19 Pa/m, and k_t = 1e10 Pa/m in sands.

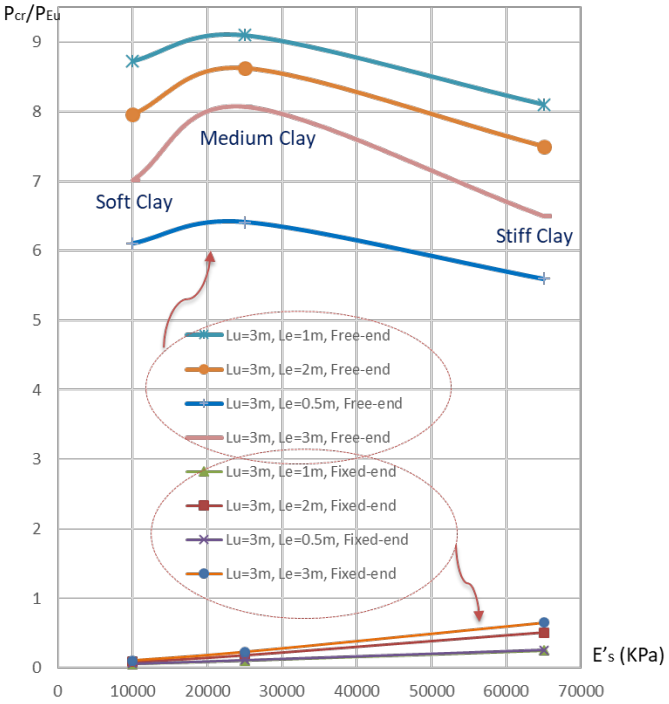

Figure 15. Buckling behaviour curves of fixed- and free-end clamped piles with interface of k_n = 1e19 Pa/m, and k_t = 1e10 Pa/m in clays.

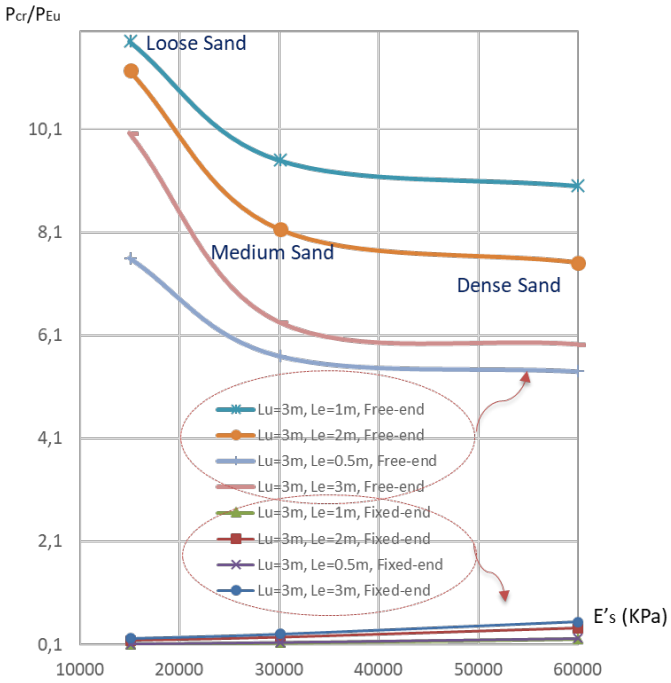

Figure 16. Buckling behaviour curves of fixed- and free-end clamped piles with interface of k_n = 1e19 Pa/m, and k_t = 1e10 Pa/m in sands.

Finally, the issue of the existence of critical depth with regards to buckling is considered. FEM results in Figs. 17 to 22 reveal its existence. The critical depth is defined as the embedded depth at which the critical buckling load is a maximum. This critical depth is present regardless of the soil type, or pile head restriction. The existence of this critical depth has important economic consequences. It is a phenomenon observed in other types of pile failures as well. Specifically, it is a well-known fact that the unit skin friction attains a maximal value at a certain depth. This could explain why a critical depth exists for pile buckling, although more studies are required to confirm this.

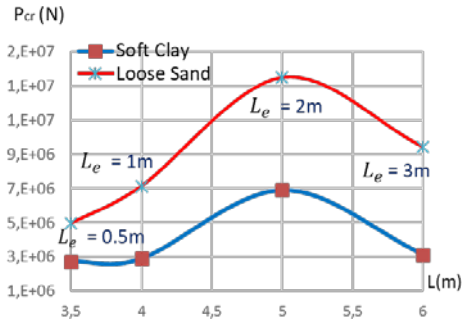

Figure 17. Critical depth for clamped piles with interface of k_n = 1e19 Pa/m, and k_t = 1e10 Pa/m in soft clay and loose sand.

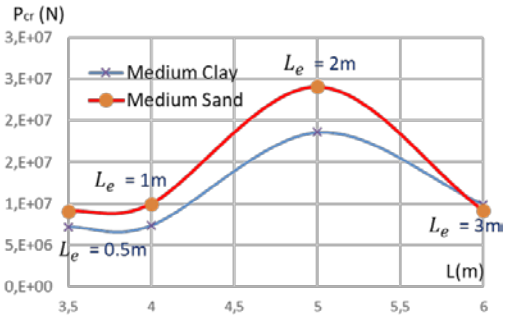

Figure 18. Critical depth for clamped piles with interface of k_n = 1e19 Pa/m, and k_t = 1e10 Pa/m in medium clay and medium sand.

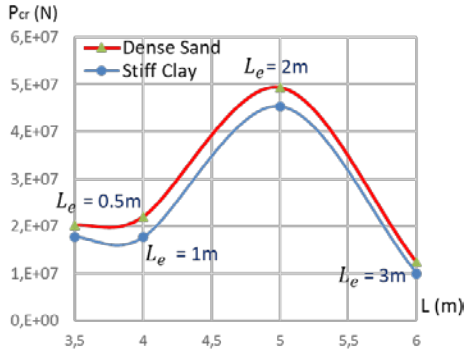

Figure 19. Critical depth for clamped piles with interface of k_n = 1e19 Pa/m, and k_t = 1e10 Pa/m in stiff clay and dense sand.

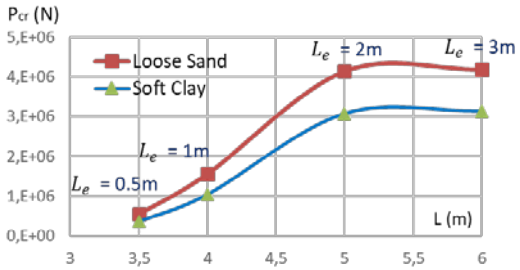

Figure 20. Critical depth for non-clamped piles with interface of k_n = 1e19 Pa/m, and k_t = 1e10 Pa/m in soft clay and loose sand.

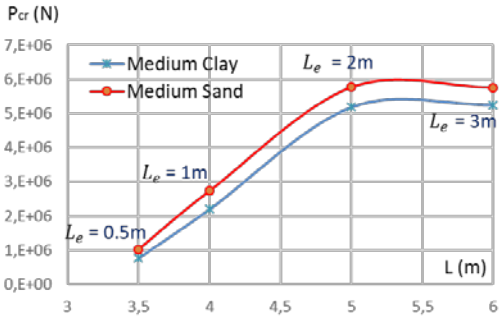

Figure 21. Critical depth for non-clamped piles with interface of k_n = 1e19 Pa/m, and k_t = 1e10 Pa/m in medium clay and medium sand.

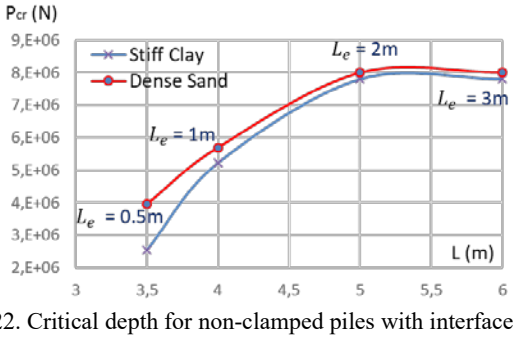

Figure 22. Critical depth for non-clamped piles with interface of k_n = 1e19 Pa/m, and k_t = 1e10 Pa/m in medium clay and medium sand.

CONCLUSION

This study brings to light important aspects the civil engineer must consider when analysing the stability of piles embedded in soils (failure by buckling). As far as modelling is concerned, the soil-pile interface plays an important

role because of its influence on the resulting critical buckling load. The value of critical buckling load, as demonstrated in this study, is very sensitive to the value of the pile-soil interface stiffness one imposes. Consequently bracketing the stiffness coefficients, between perfectly smooth and perfectly rough values is necessary in design. Even more so in the field, because the value of interface friction is not easily obtained experimentally.

The influence of the surrounding soil medium on the critical buckling load is unquestionable. In general, for similar embedment depths, interface conditions and pile head restraints, sands offer greater resistance then clays.

One must realize that if piles are constructed in potentially liquefiable soils then they should be extended all the way to bedrock. Moreover, in the advent of a seismic event, one can no longer rely on the surrounding liquefied medium for support. The pile stability is then calculated just like a typical column assuming a fixed end condition. This type of design is an exception rather than a rule.

Finally, the existence of a critical depth concerning stability of the pile is brought to light in the present study. It is clear that the surrounding soil medium confines the soil and consequently the critical buckling load increases with embedment depth. However, this increase in the critical buckling load will reach a maximum value at a particular embedment depth with no further increase, if the depth of embedment is increased. It is too early to speculate about the reasons that explain this phenomenon without experimental as well as additional numerical studies. However, the critical depth of piles, with respect to the unit skin friction, is well documented in the literature and this could be a possible reason for the existence of the critical depth with respect to stability.

REFERENCES

1. Bergfelt, A. (1957), *The axial and lateral load bearing capacity and failure by buckling of piles in soft clay*, Proc. 4th Int. Conf. Soil Mechanics and Foundation Engineering (ICSMFE), London, 1957, Vol.2, pp. 8-13.
2. Bhattacharya, S., Pile instability during earthquake liquefaction, Doctoral thesis, University of Cambridge, Cambridge, UK, 2003.
3. Bhattacharya, S., Dash, S.R., Adhikari, S. (2008), *On the mechanics of failure of pile-supported structures in liquefiable deposits during earthquakes*, Current Science J, Bangalore, 94(5): 605-611.
4. Brandtzaeg, A., Elvegaten, E.H. (1957), *Buckling tests of slender steel piles in soft, quick clay*, Proc. 4th Int. Conf. Soil Mechanics and Foundation Engineering (ICSMFE), London, 1957, Vol.2, pp.19-23.
5. COMSOL Multiphysics Reference Manual, Version 5.3, 2017.
6. Ćosić M., Folić B., Sedmak S. (2012), *Buckling analysis of 3D model of slender pile in interaction with soil using finite element method*, Struc. Integ. and Life, 12(3): 221-232.
7. Dash, S.R., Bhattacharya, S., Blakeborough, A. (2010), *Bending-buckling interaction as a failure mechanism of piles in liquefiable soils*, Soil Dyn. Earthq. Eng., 30(1-2): 32-39. doi: 10.1016/j.soildyn.2009.08.002
8. Davisson, M.T., Robinson, K.E. (1965), *Bending and buckling of partially embedded piles,* Proc. 6th Int. Conf. Soil Mech. and Foundation Eng., Montreal, 1965, Vol.2, pp.243-246.
9. Fleming, W.G.K., et al., Piling Engineering. 2nd Ed., John Wiley & Sons, London, 1992.
10. Folić, R., Folić, B., Lađinović, Đ. (2011), *Models for dynamic analysis of pile foundations in liquefiable soils*, 11th Int. Sci. Conf. VSU 2011, Eds. T. Tsenkov, D. Partov, Bulgaria, Vol.1, pp.228-233.
11. Golder, H.Q., Skipp, B.O. (1957), *The buckling of piles in soft clay*, Proc. 4th Int. Conf. Soil Mech. Found. Eng. (ICSMFE), London, 1957, Vol.2, pp.35-39.
12. Haldar, S., Sivakumar Babu, G.L. (2010), *Failure mechanisms of pile foundations in liquefiable soil: Parametric study*, Int. J Geomechanics, 10(2): 74-84.
13. Kumar, S., Karuppaiah, B., Parameswaran, P. (2007), *Buckling behavior of partially embedded reinforced concrete piles in sand*, ARPN J Eng. Appl. Sci., 2(4): 22-26.
14. Nadeem, M. Chakraborty, T., Matsagar, V. (2015), *Nonlinear buckling analysis of slender piles with geometric imperfections*, J Geotech. Geoenviron. Eng., 141(1). doi: 10.1061/(ASCE)GT.1943-5606.0001189
15. Poulos, H.G., Davis, E.H., Pile Foundation Analysis and Design, Rainbow-Bridge Book Co, 1980.